Polymer 223 (2021) 123664

Contents lists available at ScienceDirect

Polymer

journal homepage: http://www.elsevier.com/locate/polymer

Investigating the role of polymer size on ionic conductivity in free-standing hyperbranched polyelectrolyte membranes

Tobias Abrahamsson [a], Mikhail Vagin [a], Maria Seitanidou [a], Arghyamalya Roy [a], Jaywant Phopase [a], Ioannis Petsagkourakis [a], Nathalie Moro [a,b], Klas Tybrandt [a], Xavier Crispin [a], Magnus Berggren [a], Daniel T. Simon [a,*]

[a] Laboratory of Organic Electronics, Department of Science and Technology, Linköping University, 601 74, Norrköping, Sweden
[b] Empa, Swiss Federal Laboratories for Materials Science and Technology, Laboratory for Biointerfaces, 9014, St. Gallen, Switzerland

ARTICLE INFO

Keywords:
Ion-exchange membrane
Polymer size dependant ionic conductivity
Hyperbranched polyelectrolyte
Multi-functionalization
Click cross-linking

ABSTRACT

Polymer-based ion exchange membranes (IEMs) are utilized for many applications such as in water desalination, energy storage, fuel cells and in electrophoretic drug delivery devices, exemplified by the organic electronic ion pump (OEIP). The bulk of current research is primarily focused on finding highly conductive and stable IEM materials. Even though great progress has been made, a lack of fundamental understanding of how specific polymer properties affect ionic transport capabilities still remains. This leads to uncertainty in how to proceed with synthetic approaches for designing better IEM materials. In this study, an investigation of the structure-property relationship between polymer size and ionic conductivity was performed by comparing a series of membranes, based on ionically charged hyperbranched polyglycerol of different polymer sizes. Observing an increase in ionic conductivity associated with increasing polymer size and greater electrolyte exclusion, indicating an ionic transportation phenomenon not exclusively based on membrane electrolyte uptake. These findings further our understanding of ion transport phenomena in semi-permeable membranes and indicate a strong starting point for future design and synthesis of IEM polymers to achieve broader capabilities for a variety of ion transport-based applications.

1. Introduction

Ion exchange membranes (IEMs) are a key component in a wide variety of technologies due to their ability to selectively conduct ionic species of a given electrical polarity [1]. The phenomena has been utilized in applications including fuel cells and electrochemical devices [2], electrodialysis [3], water purification [4], energy storage [5], and organic electronics [6]. Ion transport and signaling are also fundamental functions in living organisms and a variety of "iontronic" technologies based on IEMs, such as the organic electronic ion pump (OEIP), have thus been developed to bridge the gap between biology and technology via targeted electrophoretic delivery of ionic substances, *e.g.*, for therapeutic or biological applications [7–15]. There is thus a growing interest across several disciplines in understanding and developing more efficient and high-performing IEMs and their dependent technologies. An IEM generally comprises an insoluble polymeric structure with either fixed anionic or cationic charges covalently bound to the polymeric backbone with associated free counterions (opposite charge as the fixed membrane charges). The free counterions can thus be exchanged and transported through the IEM by applying an electrical potential while prohibiting the passage of co-ions (same charge as fixed membrane charges), an effect known as Donnan exclusion [16]. IEMs with fixed anion charge and mobile cationic counterions are referred to as cation exchange membranes (CEMs) and IEMs with fixed cation charge and mobile anionic counterions are referred to as anion exchange membranes (AEMs).

Most of today's research efforts on IEMs focus on highly involved processing techniques with commercially available materials for performance optimization but generally lack deeper elucidation of the ion exchange phenomena. This is primarily due to the general complexity and subtle variations of the materials and systems that are studied and explored. However, studying physical parameters such as conductivity, fixed charge concentration, etc., are useful metrics for comparison and lend themselves to structure-property investigations. The vast majority

* Corresponding author.
E-mail address: daniel.simon@liu.se (D.T. Simon).

https://doi.org/10.1016/j.polymer.2021.123664
Received 10 November 2020; Received in revised form 9 March 2021; Accepted 14 March 2021
Available online 23 March 2021

of IEMs have been synthesized based on monomer or co-monomer units directly polymerized (and cross-linked, *e.g.*, by heating) into membranes or by post-functionalization of membranes by chemical treatment to introduce charge [17]. Such IEMs have seen great success in various applications, but it is challenging to gain insight into their chemical structural arrangment. Furthermore, for linear polymers the challenge in structural elucidation is exacerbated by the many possible structural configurations the polymers can adopt. An alternative to linear polymer-based IEMs is hyperbranched polymer-based materials, which can result in more consistent structures and thus lend themselves to more systematic structure-property studies.

Hyperbranched polymers consist of a category of polymers with an intrinsic structural arrangement based on branching covalent bonded network, see Fig. 1. In turn the overall polymer structure configuration is more limited by its covalent bonds. These materials have many of the characteristics of dendritic polymers but have viable synthetic approaches for large-scale application even beyond pharmaceuticals [18]. Recently, hyperbranched polyglycerols (HPGs) have been explored as IEM materials in iontronic devices [12,19–23]. These studies indicated that HPG-based IEM's are promising for their anionic and cationic conductivity [20,21,23], synthetic versatility pre-cross-linking [19,20], UV click cross-linking [12,19,20], a typically improved stability when comparing to linear counterparts [22], and a manifold of application areas [12,19,20,23]. However, like linear polymer-based IEMs, a detailed understanding of the dependence of performance on material structure remains to a large extent unknown. Here we study the IEM properties of HPGs by investigating the role of polymer size on ionic conductivity to shed more light on HPG-based IEMs and IEMs in general. Three different HPG polymer sizes of 2.5, 5, and 10 kDa were here explored, with molecular weight and degree of branching characterized to ensure that contributing differences were based primarily on polymer size. HPGs were multi-functionalized into hyperbranched polyelectrolytes with controlled amounts of charged groups and available cross-linking groups, enabling the fabrication of free-standing AEMs and CEMs. Our essential conclusion is that larger polyelectrolytes provide an increased ionic conductivity and fixed charge concentration without compromising selectivity or increasing swelling/hydration. These findings hope to further the understanding of ion-exchange phenomena and provide a templet for synthetic design of new generations of polyelectrolytes. We also demonstrate these hyperbranched polyelectrolyte-based membranes as having large molecular ionic transportation capabilities, an important aspect in the field of organic bioelectronics.

2. Experimental

2.1. Materials

Hyperbranched polyglycerol (HPG) of 2.5, 5, and 10 kDa were purchased from NanoPartica GmbH. Reference 10 kDa HPGs were synthesized in-house and in parallel by RISE (Research Institutes of Sweden, Södertälje), with molecular weight based on GPC and ^{1}H NMR analysis (details below). Bruno Bock Chemische donated Thiocure ETTMP 1300.

2.2. Instruments and software

NMR analysis was performed with an Inova Varian Oxford AS500 (500 MHz) spectrometer utilizing an internal solvent peak for reference [24]. Acquired free induction decay (FID) data was processed with MestReNova 12.04–22023 (Mestrlab Research). Electrochemical impedance measurements were performed using a BioLogic SP200 potentiostat and data analyzed with EC Lab 11.20 software. A Keithley 2602 SourceMeter (Keithley Instruments) with custom-designed LabVIEW (National Instruments) software was used for direct current electrochemical characterization. Dynamic light scattering (DLS) was performed using an ALV-CGS-5022F goniometer system (ALV GmbH, Langen) with a 22 mW 633 nm HeNe laser in pseudo-cross-correlation mode, with scattered light collected into a single-mode optical fiber and split to two avalanche photodiodes (PerkinElmer). The time-correlation function of the scattered intensity was obtained by a dual multiple-tau correlator with 328 channels (ALV-6010-160) and a constrained regularization method (CONTIN, supplied with the correlator software) was used to calculate correlation time distributions. These were in turn converted into size distributions via the Stokes-Einstein relationship [25]. UV–Vis spectra were recorded with an Lambda 900 absorption spectrometer (PerkinElmer).

2.3. Synthesis and characterization of hyperbranched polyglycerols

Hyperbranched polyglycerol (target M_w =10 kDa) was synthesized (Scheme 1 and Supporting Information) and characterized according to literature [26].

2.3.1. Inverse gated ^{13}C NMR (degree of branching)

Samples were prepared with 30 mg HPG sample in 0.7 mL DMSO-d_6. 2 sec relaxation delay between scans and number of scans 16,384 for the NMR analysis.

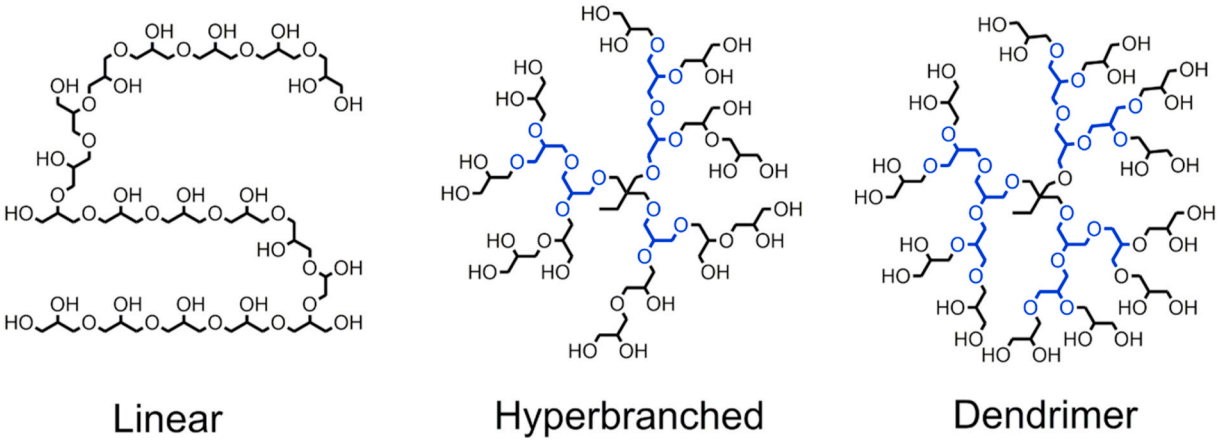

Fig. 1. Illustrative representation of different polyglycerols structures (~1.3–1.7 kDa). The hyperbranched and the dendrimer polyglycerols displays dendritic (blue) structure. Dendritic polymers have a 100% degree of branching (dendritic structure) and in comparison, the displayed hyperbranched polymer has 55.6%. The linear polymer contains no dendritic structure and can adopt a wide variety of conformations while hyperbranched and (to an even higher extent) dendritic structures are restricted in their macromolecular structure. (For interpretation of the references to color in this figure legend, the reader is referred to the Web version of this article.)

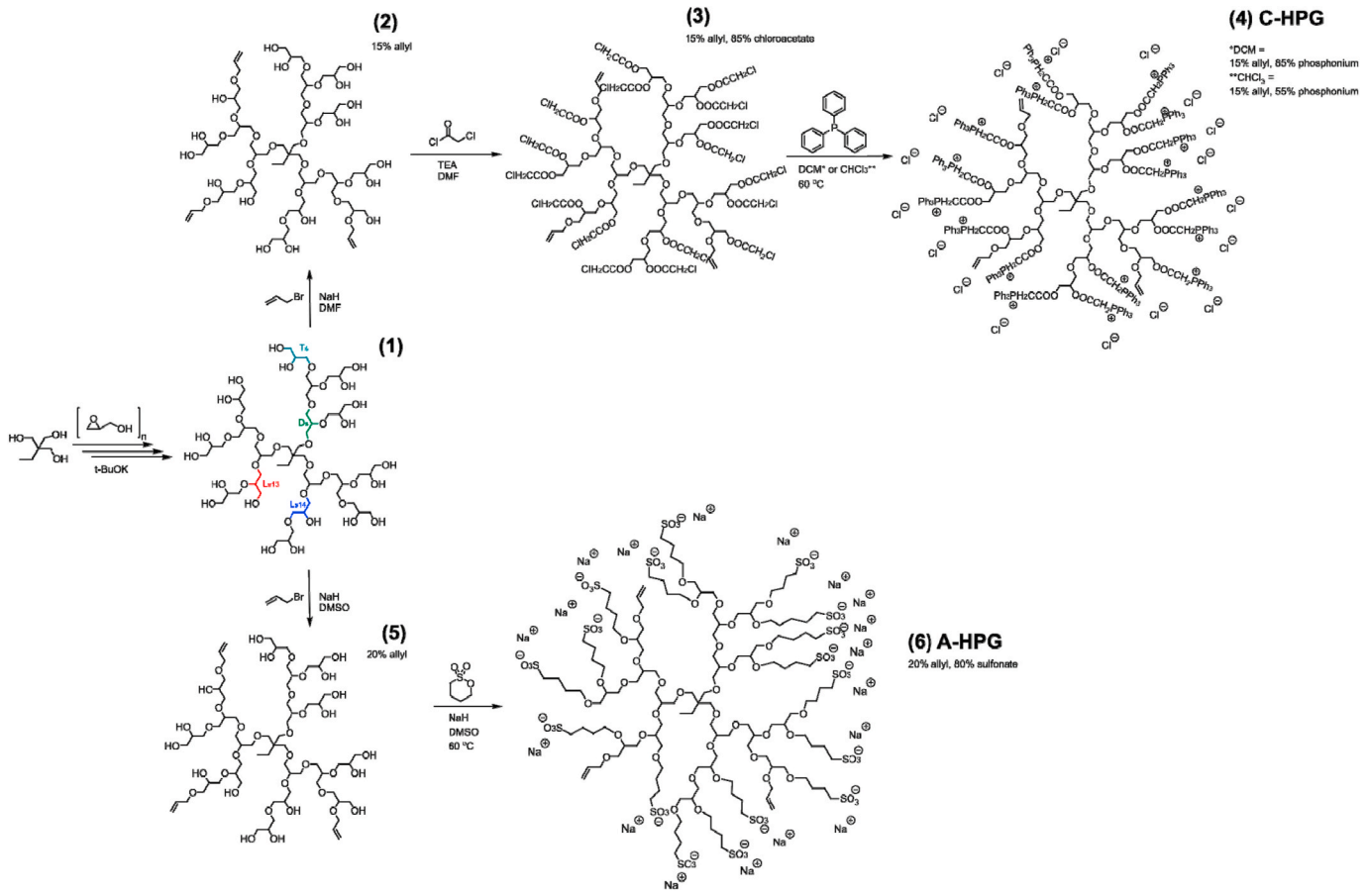

Scheme 1. Synthesis of hyperbranched polyglycerol (HPG, **1**), allyl-HPG with various amounts of allyl functionalization (**2** and **5,** 15% resp. 20%) and multi-functionalization into allyl-chloroacetate-HPG (**3**), 85% functionalized cationic charged C (85)-HPG (**4***), 55% C (55)-HPG (**4****) and 80% functionalized anionic charged A (80)-HPG (**6**). For C (55)-HPG chloroform is used as solvent in the last step of the synthesis while for C (85)-HPG dichloromethane is used. The illustrated structures does not represent the full sized structures of the reported polymers and polyelectrolytes (which can be up to 6–7 times larger) and with hyperbranched structure (with 45–60% dendricity).

2.3.2. Gel permeation chromatography

Molecular weight (M_w), number-average molar mass (M_n), max molecular weight peak (M_p), and polydispersity index (PDI) determination was performed by gel permeation chromatography (GPC) with an HPLC-system equipped with a column oven, mobile phase degasser, and a RI-detector cell operated at 30 °C. The pre-column was a Suprema (5 μm, 8 × 50 mm) and the analytical column a Suprema 100 Å (5 μm, 8 × 300 mm, Polymer Standards Services) with the column temperature set to 25 °C. The mobile phase for separation was $NaNO_2$ (aq, 10 mM) with a flow rate set to 1 mL/min and calibrations were performed using linear pullulan standards (342–47100 Da, Polymer Standards Services). The sample injection volume was 20 μL with 10 mg/mL concentration HPG sample and an analysis run time of 15 min.

2.4. Synthesis of multi-functionalized ionic hyperbranched polyglycerols - dendrolytes

Cationic HPG (C (55)-HPG and C (85)-HPG) based on 2.5, 5, and 10 kDa HPG were synthesized (Scheme 1, Supporting Information) according to a previously published protocol [19]. Anionic HPG (A (80)-HPG) based on 5 and 10 kDa HPG were synthesized (Scheme 1, Supporting Information) according to a previously published protocol [20].

2.5. Dynamic light scattering (DLS) sample preparation

Samples were prepared using 200 mg of C (85)-HPG2.5, 5, or 10 (Scheme 1 (4*)), allyl (15%)-triphenylphosphoniumacetate (85%)-HPG 2.5, 5, or 10 kDa) were dissolved in 2 mL water (0.1 mg/mL), filtered through a 0.45 μm PVDF membrane, and introduced into 10 mm diameter cylindrical cuvettes. The cuvettes were immersed in a refractive index-matching toluene bath at a controlled temperature of 22 ± 0.02 °C.

2.6. Cross-linking (free-standing membranes)

Thermal and photo-initiated cross-linking of A-HPG and C-HPG has previously been reported by our group [19,20] with a process mediated by the HPGs' allyl functionality combined with a thiol-based (functionalized polyethylene glycol) cross-linking agent (Thiocure ETTMP 1300) in a thiol-ene click reaction [27–29]. Here, the polyelectrolyte membrane solutions were cast on a Teflon surface and subsequently UV-cured (Figure S14) with one of several formulations of C-HPG or A-HPG polymer and thiol-based cross-linker: one with a high amount of cross-linker (F1) 1:1 w/w C-HPG/Thiocure, one with low amount of cross-linker (F2) 2.9:1 w/w C-HPG/Thiocure, and a single A-HPG formulation of 2.4:1 w/w A-HPG/Thiocure. Details follow.

2.6.1. C(55)-HPG formula 1 (F1)

1,3,5-Triallyl-1,3,5-triazine-2,4,6(1H,3H, 5H)-trione (7.9 mg), 2-hydroxy-4′-(2-hydroxyethoxy)-2-methylpropiophenone (10.2 mg), Thiocure ETTMP 1300 (150 mg), and C (55)-HPG 2.5, 5, or 10 kDa ((Scheme 1 (4**)), 150 mg) were dissolved in methanol (300 μL) by vortex and sonication for 5 min. The homogenous solution was drop-cast

onto a Teflon substrate to fill Parafilm molds (1 mm thickness, 8 mm Ø) and UV cross-linked for 30 min with a Süss MA/BA6 mask aligner (flood exposure, 2 mW/cm^2 measured at 365 nm).

2.6.2. C(55)-HPG formula 2 (F2)

1,3,5-Triallyl-1,3,5-triazine-2,4,6(1H,3H, 5H)-trione (4.7 mg), 2-hydroxy-4′-(2-hydroxyethoxy)-2-methylpropiophenone (3.5 mg), Thiocure ETTMP 1300 (34.7 mg), and C (55)-HPG 2.5, 5, or 10 kDa (Scheme 1, (4**)), 100 mg) were dissolved in methanol (50 μL) by vortex and sonication for 5 min. The homogenous solution was drop-cast onto a Teflon substrate to fill Parafilm molds (1 mm thickness, 8 mm Ø) and UV cross-linked for 30 min with a Süss MA/BA6 mask aligner (flood exposure, 2 mW/cm^2 measured at 365 nm).

2.6.3. C(85)-HPG formula 2 (F2)

1,3,5-Triallyl-1,3,5-triazine-2,4,6(1H,3H, 5H)-trione (4.7 mg), 2-hydroxy-4′-(2-hydroxyethoxy)-2-methylpropiophenone (3.5 mg), Thiocure ETTMP 1300 (34.7 mg), and C (85)-HPG 2.5, 5, or 10 kDa ((Scheme 1 (4*)), 100 mg) were dissolved in methanol (50 μL) by vortex and sonication for 5 min. The homogenous solution was drop-cast onto a Teflon substrate to fill Parafilm molds (1 mm thickness, 8 mm Ø) and UV cross-linked for 30 min with a Süss MA/BA6 mask aligner (flood exposure, 2 mW/cm^2 measured at 365 nm).

2.6.4. A(80)-HPG formula

2-Hydroxy-4′-(2-hydroxyethoxy)-2-methylpropiophenone (2 mg), Thiocure ETTMP 1300 (83 mg), A (80)-HPG 5 or 10 kDa (Scheme 1 (6), 200 mg) were dissolved in water (62 μL) and methanol (124 μL) by vortex and sonication for 1 min. The homogenous solution was drop-cast onto a Teflon substrate to fill Parafilm molds (1 mm thickness, 8 mm Ø) and UV cross-linked for 30 min with a Süss MA/BA6 mask aligner (flood exposure, 2 mW/cm^2 measured at 365 nm).

2.6.5. Free-standing membrane thickness

Thickness was measured with a Digimatic Micrometer MDH-25 M (Mitutoyo) near the center of casted membrane. Each membrane was measured 5 times and the calculated average thickness was used.

2.7. Electrochemical impedance spectroscopy (EIS) – indirect method [30]

Prior to measurement, free-standing membranes were washed and equilibrated in 0.05 M NaCl (aq) for 2 h and the electrolyte solution was exchanged three times. Electrochemical impedance spectroscopy (EIS) was performed using a custom two-reservoir H-cell (7 mL electrolyte on each side), where the membrane was mounted at a circular hole with an effective area of 0.196 cm^2 connecting the two reservoirs (Fig. 2). Two titanium electrodes were used with an effective area of 2.6 × 2.6 cm each, submerged in the electrolyte solution, and were at each side of the membrane in their respective reservoirs. The distance between the electrodes were 6 mm (total) and 2.5 mm each to the membrane interface. The membrane was allowed to reach equilibrium with each electrolyte tested and any signs of leakage were checked for. Measurements were performed in the frequency range 1 Hz–100 kHz with an applied sinusoidal amplitude of 10 mV until stable impedance was reached. The background resistance of the H-cell setup without any membrane was subtracted from the resistance values with the membrane mounted. For C (55)-HPG F1 and F2, three different membranes of each formulation were measured, based on 2.5, 5, and 10 kDa HPG. C (85)-HPG 2.5, 5, or 10 kDa F2 were one membrane measured for each size. Two membranes each of A-HPG membranes based on 5 and 10 kDa HPG were measured. The standard curve (without membrane) was the average values obtained from four different measurements with separately prepared electrolyte solutions of 0.01, 0.05, 0.075, 0.1, 0.2, 0.4, 0.5, 0.6, 0.75, 1, 1.5 and 2 M NaCl.

2.8. Direct current measurements (conductivity and selectivity)

Membrane permselectivity and relative conductivity characterization of C (55)-HPG2.5, 5, and 10 F2 and C (55)-HPG5 F1 membranes were performed using the custom H-cell (Fig. 2) with two platinum gauze 80 mesh (35 × 25 mm) electrodes placed 22 mm apart from each other, with 10 mm to membrane interface. The target system was grounded and a constant potential of 1 V was applied to the platinum source electrode. Current was recorded (with a Keithley 2602 SourceMeter, custom LabVIEW) between the source and target until reaching a stable level. The membrane selectivity was studied with different concentrations for the source reservoir (7 mL) of 10, 50, 100, 200, and 400 mM NaCl (aq) electrolyte and a fixed target reservoir (7 mL) of 10 mM NaCl (aq). The membranes were also tested with varied target electrolyte of 10 mM KCl, NaCl, or salicylic acid with constant source electrolyte (400 mM NaCl).

2.9. Alizarin Red S transport (four-probe H-cell)

A four-probe H-cell setup was used for transportation and release of Alizarin Red S across a C (55)-HPG5 F1 membrane (area: 0.196 cm2, thickness: 0.05 cm). The source electrolyte was an Alizarin Red S (Fig. 3) solution (58.44 mM (aq), 7 mL) and the target electrolyte was NaCl (0.1 M (aq), 7 mL). A constant current (3 mA) was applied using a BioLogic SP200 potentiostat between the working and counter electrodes (platinum gauge) with the reference electrodes on each side (Ag/AgCl, placed close to the membrane interface) recording the potential (Figs. S21-22). Target electrolyte samples were collected (after 33 min). Passive diffusion control was performed after adding new Alizarin Red S and NaCl solutions in the source and target reservoir, respectively. The target reservoir sample was collected after 16 h. Sampled Alizarin Red S concentrations were determined via UV–Vis spectroscopy and

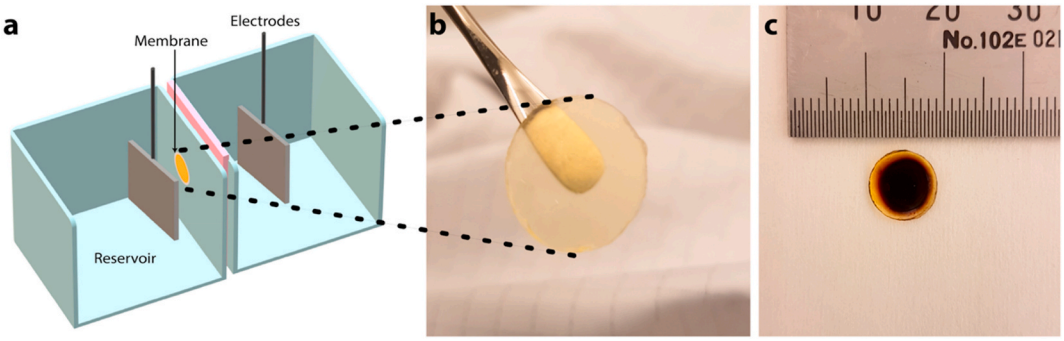

Fig. 2. Electrochemical characterization setup. (a) H-cell for (b) free-standing membrane. (c) Alizarin Red S (342.25 g/mol) previously transported and released through a cationic hyperbranched polyglycerol membrane (C (55)-HPG5 F1, with dark red/black dye coloration) and membrane dimension displayed. (For interpretation of the references to color in this figure legend, the reader is referred to the Web version of this article.)

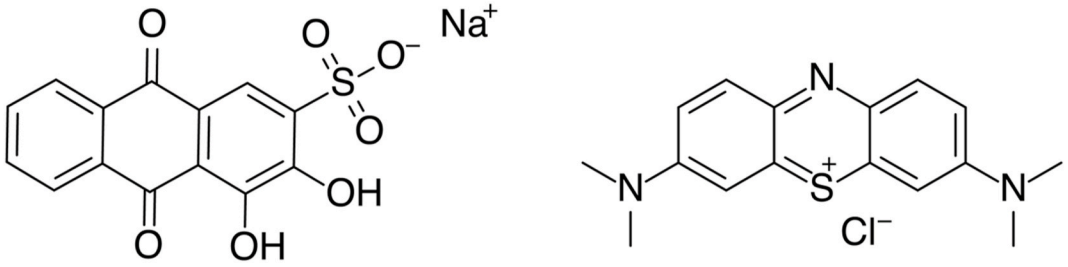

Fig. 3. Alizarin Red S (left, 342.25 g/mol) and methylene blue (right, 319.85 g/mol).

absorption at 260 nm. Reference Alizarin Red S concentrations of 9.77, 19.53, 39.06, 78.13, and 156.25 μM were measured in 0.1 M NaCl to establish the standard curve.

2.10. Organic electronic ion pump fabrication (OEIP)

OEIPs were fabricated using micro-molding in capillaries (MIMIC) [31] as previously reported [19] (Figure S18). The master mold was prepared by photolithographically patterning 27 μm wide × 12 μm high lines of spin-coated SU-8 3050 (MicroChem Corp.) on silicon/silicon dioxide substrates. Sylgard 184 (Dow Chemical) was used to prepare the PDMS solution by mixing the oligomer (silicone elastomer base) and a radical initiator (curing agent) in a 10:1 ratio. A centrifuge system was used to de-gas the mixture which was then poured onto the master mold and annealing overnight at 60 °C. The PDMS mold was carefully removed from the master and laser-cut into sheets, with 5000 μm (length) capillary channels connecting two electrolyte reservoirs (0.5 cm × 0.5 cm, Figure S18). The PDMS sheets and pre-cleaned glass substrates were then kept in a Zepto W6 plasma cleaner (Diener, Germany) for 5 min at 50 W followed by bonding via annealing. Resulting micro-channels were then filled by capillary force with either solutions of:

2.10.1. A(80)-HPG formula capillary

2-Hydroxy-4′-(2-hydroxyethoxy)-2-methylpropiophenone (3.4 mg), Thiocure ETTMP 1300 (13 mg), and A (80)-HPG 5 or 10 kDa (Scheme 1 (6), 40 mg) dissolved in water (50 μL) and methanol (50 μL).

2.10.2. C(55)-HPG formula 2 capillary

1,3,5-Triallyl-1,3,5-triazine-2,4,6(1H,3H, 5H)-trione (10.4 mg), 2-hydroxy-4′-(2-hydroxyethoxy)-2-methylpropiophenone (4.6 mg), Thiocure ETTMP 1300 (52 mg), and C (55)-HPG 2.5, 5, or 10 kDa (Scheme 1 (4**)), 208 mg) dissolved in methanol (200 μL) and water (440 μL).

2.10.2.1. Capillary cross-linking. Filled MIMIC devices were then cross-linked for 15 min with UV 254 nm, 0.2 mW/cm.

2.10.3. OEIP DC characterization

OEIP devices were characterized using DC measurements (Keithley 2602 SourceMeter, custom LabVIEW) using source and target electrodes each comprising PEDOT:PSS on a PET substrate (Orgacon F-350 film; AGFA-Gevaert) with a layer of carbon paste applied at the metallic connector contacts. A constant 3 V potential was applied between source and target reservoirs, each filled with 100 mM NaCl(aq) until reaching stable currents. Membrane fixed charge concentration measurements were performed by switching the source electrolyte with either 100 mM NaBr for CEM or 100 mM LiCl for AEM and the ionic exchange displacements were recorded until reaching stable current levels.

2.10.4. Methylene blue transportation

Using an OEIP filled with A (80)-HPG 10 kDa (formula capillary), methylene blue transportation was characterized by filling the source reservoir with 10 mM methylene blue (aq.) (Fig. 3) and the target reservoir with 10 mM KCl solution and applying a constant 3 V potential between the source and target (see OEIP DC characterization setup).

2.11. Degree of swelling

Membranes were equilibrated in 0.1 M NaCl (aq) and then soaked in deionized water for 4 h, changing the solvent every hour. Dry mass was then measured after drying the membranes in an oven for 4 h at 70 °C. The membranes were subsequently equilibrated in 0.1, 0.5, or 1 M NaCl (aq) for at least 3 h and weighed between the electrolyte concentration changes (excess surface water quickly wicked off with a tissue prior to weighing). 3 h equilibration was deemed sufficient based on ~30 min equilibration during solution changes in the EIS experiments. The average masses were taken from four different membranes of each series.

3. Results and discussion

In this study, the hyperbranched polyelectrolyte materials synthetized (Scheme 1) were based on functionalization of commercial HPGs of different sizes (2.5, 5, 10 kDa), with a degree of branching (DB) of average 50% (±4) (dendricity) as well as custom-synthesized [26] HPGs with up to 59–60% DB and lower polydispersity. The in-house reproduced custom-synthesis thus confirmed the reproducibility of slow monomer addition for the ring-opening multi-branching polymerization (ROMBP) reaction [32,33], though under ideal conditions [34,35] the expected DB could reach up to 66%. While not achieving perfect dendritic symmetry (*i.e.*, 100% DB), this approach makes up for the costly procedure of dendrimer polymer synthesis while still obtaining a high degree of dendricity in the structure.

3.1. HPG molecular weight analysis

Molecular weights for variously sized HPGs were measured using ^{1}H NMR polymer molecular weight analysis [36]. Proton integral intensity of the distinct single moieties from the core molecule (trimethylolpropane, α-3H and β-2H) were compared to the bulk signal of the repeating polymer units of HPG shown in Fig. 4 leading to a calculation [36] of the molecular weight $M_{w,poly}$:

$$M_{w,\,poly} = \left(\frac{i_x p_y n_y}{i_y p_x}\right) x\, M_{w,\,mono} + M_{w,core} \quad (1)$$

where i_x is the ^{1}H NMR integral of the repeating polymer units, i_y is the core unit integral (α or β), p_x and p_y are the number of protons represented by each moiety (5H and 3H/2H, respectively), and n_y is the number of repeating units of y (= 1). The first expression of Eqn. (1) is equivalent to the number of monomer units (n_{mono}). By multiplying this expression with the monomer molecular weight ($M_{w,mono}$, 74.08 g/mol) and then adding of the core unit molecular weight ($M_{w,core}$, 131.15 g/mol), M_w can be obtained. Data from ^{1}H NMR polymer molecular weight analysis of 2.5, 5, and 10 kDa HPGs are shown in Fig. 4 and summarized in Table 1. Since HDO peak presence in the HPG region influences integral intensity due to DMSO-d_6, ^{1}H NMR performed in D_2O solvent was

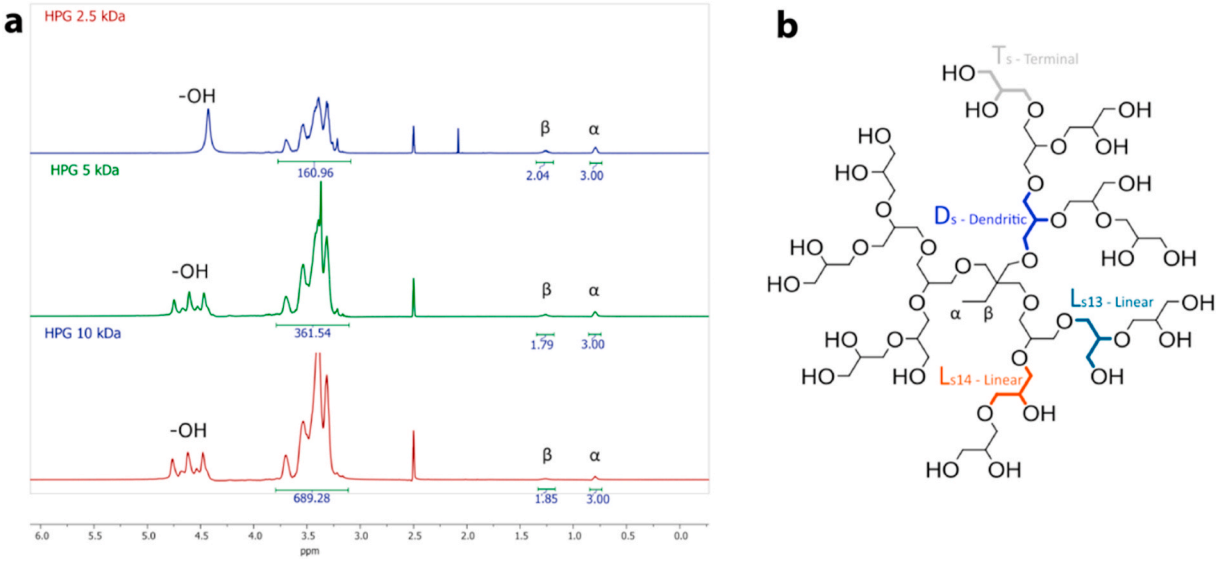

Fig. 4. (a) ^{1}H NMR (DMSO-d_6) of 2.5, 5, and 10 kDa Hyperbranched Polyglycerols (HPGs). Integral region 4.00–3.00 ppm corresponds to the polymer bulk signal and 1.40–1.15 and 0.85–0.65 ppm to the single-core moieties from trimethylolpropane, (b) with methylene (β, 2H) and methyl (α, 3H), respectively. Dendritic, linear, and terminal subunits of HPG.

Table 1
Hyperbranched Polyglycerol (HPG) of 2.5, 5 and 10 kDa samples analyzed by NMR and GPC. Hydroxyl groups (OH) per polymer, molecular weight (M_w) poly, number average molar mass (M_n), peak molecular weight (M_p), dispersity index (PDI) and degree of branching (DB).

	^{1}H NMR (D_2O) *OH groups/polymer*	^{1}H-NMR (D_2O) M_w	^{1}H-NMR (DMSO-d_6) M_w	GPC M_w	GPC M_n	GPC M_p	GPC PDI	IG ^{13}C-NMR ($D_1 = 2$ s, DMSO-d_6) *DB*
HPG 2.5 kDa	31.5	2461	2516	2188	982	2461	2.51	46.1%
HPG 5 kDa	65.9	5011	5488	5448	1461	5836	3.73	49.5%
HPG 10 kDa	120.1	9028	10,344	9891	4508	9977	2.19	53.4%
HPG 10 kDa Ref. 1 Crude	123.2	9259	9364	7943	2847	9173	2.79	50.3%[a]
HPG 10 kDa Ref. 1	117.2	8811	9100	9049	5585	9309	1.62	59.4%
HPG 10 kDa Ref. 2			9031	9356	5274	9147	1.77	60.0%

[a] $D_1 = 1$ s.

also reported (Table 1 and Figure S1-2).

Molecular weights were then ascertained using gel permeation chromatography (GPC) accordingly to a previously reported method for HPGs [26]. The data are summarized in Table 1 (and chromatograms reported in Fig. 4S). GPC-derived weights are in good agreement with the ^{1}H NMR results. ^{1}H NMR polymer weight analysis is incapable of elucidating poly dispersity and discriminating of smaller polymer particles contributions and could thus result in higher estimated polymer size. This was indeed observed when comparing the HPG10 Ref. 1 Crude (pre-purification) sample to HPG10 Ref. 1 (post purification). With ^{1}H NMR analysis, the crude sample exhibited a slightly higher M_w compared to the purified samples. However with GPC, M_w, the number-average molar mass (M_n) and the peak molecular weight (M_p) can be distinguished to showcase that the overall M_w was actually lower for the crude sample. On the other hand, due to a lack of well-established GPC standards for water-soluble hyperbranched polymers [26], using linear standards could lead to an overestimation of the molecular weights, therefore justifying a combination of both techniques for proper clarification. Overall, the molecular weight of the main samples HPG 2.5, 5, and 10 kDa could be clearly established even with differences in the polydispersity index (PDI). HPG10 Ref. 1 and 2 showcase samples from two different syntheses along with reproducible results from both analyses.

3.2. HPG degree of branching

A crucial aspect of hyperbranched polymer structure is the degree of branching (DB). With inverse gated (IG) ^{13}C NMR, the DB could be elucidated in the various HPGs. The ^{13}C NMR spectra of HPGs' structural subunits have previously been reported [26,32,37,38] and the DB can be derived from Ref. [32]:

$$DB = \frac{2D_s}{2D_s + L_{s13,\ s14}} \quad (2)$$

where L_{s13} corresponds to linear units where propagation occurred on secondary hydroxyl groups while L_{s14} on primary, D_s dendritic and T_s indicates terminal units (Fig. 4b). Values obtained with IG ^{13}C NMR for the 2.5, 5 and 10 kDa HPG series (Fig. 3S) are summarized in Table 1. DB 49.7 ± 3.7% indicates very similar amount of branching/dendricity between the different seized HPGs. Our own synthesized HPG Ref. 1 and Ref. 2 reliably resulted in a DB/dendricity of 59–60%. The final dialysis purification performed on HPG Ref. 1 and Ref. 2 not only contributes to lower PDI, but may also contribute to the higher DB. It is important to note that most of the IG ^{13}C NMR analyses were performed with a set relaxation delay of $D_1 = 2$ s between pulses while standard ^{13}C NMR uses $D_1 = 1$ s. The lower DB of HPG Ref.1 Crude (50.3%) may be attributed to the lower pulse delay, but a comparison can be made between the purified samples HPG Ref. 1 and 2, which were run with $D_1 = 1$ s (51.0% and 51.9% DB, respectively) and $D_1 = 2$ s (59.4% and 60.0%,

respectively, Table 1). Here, the increase in DB with a 1 s increase in delay time is approximately 9%. To investigate if an even longer delay time was required for the IG ^{13}C NMR in determining the DB, the HPG 10 kDa was analyzed over three separate times using $D_1 = 1$, 2, and 8 s, resulting in 46.8%, 53.4%, and 54.6% DB, respectively. Due to the long run time with $D_1 = 8$ s and a modest +1.2% increase in DB (between $D_1 = 2$ s and 8 s), we deemed it unnecessary to measure with such accuracy. The more significant increase in resolution was achieved by increasing D_1 from 1 to 2 s, giving a +6.6% increase in DB (46.8%–53.4%). In summary, the actual values of DB may be assumed to lie around +1–2% higher than those reported in Table 1. Therefore, for efficient general characterization of DB, the found $D_1 = 2$ s at 126 MHz (Fig. 3S) for ^{13}C NMR was deemed to be optimal.

3.3. Functionalization into dendrolytes

Terminally charged hyperbranched polymer (and dendrimer, herein referred to as "dendrolyte") synthesis and structural characterization have previously been reported [19] for A-HPG and C-HPG as well as their successful and high-performing utilization in electrophoretic drug delivery devices [20]. Scheme 1 illustrates the multi-functionalization of 2.5, 5, and 10 kDa HPGs by partially functionalized allyl-groups using nucleophilic substitution and subsequent conversion of the remaining hydroxyl groups with the anionic or cationic charged groups. The degree of functionalization (DF) was determined via ^1H NMR and calculated by Ref. [19]:

$$DF(\%) = \frac{H_{func}/H_{ref}}{n_{func}/n_{ref}} \times 100 \quad (3)$$

where H_{func} and H_{ref} indicate chemical shift integrals for the funcationalized groups and reference (non-functionalized) HPGs core structure, and n_{func} and n_{ref} represent the number of protons for each group. Fig. 5 demonstrates the ^1H NMR spectra of C-HPG 10 and A-HPG 10, the general characteristics of which were also observed for the full series of 2.5, 5, and 10 kDa multi-functionalized HPGs (calculated values summarized in Table 2, full spectra in Supporting Information Figs. 6S–13). Table 2 lists the DF for the various materials based on the ^1H NMR spectrum integration and Eqn. (3). Two series of C-HPG were

Table 2
Degree of functionalization, functional groups/polymer, and polymer size (M_w) for functionalized 2.5, 5, and 10 kDa HPGs; C-HPGs (cationic) and A-HPGs (anionic) via ^1H NMR.

	Allyl groups (%)	Anionic/cationic groups (%)	Functional groups/polymer	M_w g mol^{-1}
C (55)-HPG2.5	16	56	38.8	11,377
C (55)-HPG5	16	57	74.7	21,889
C (55)-HPG10	13	56	135.8	39,583
C (85)-HPG2.5	14	85	31.7	11,666
C (85)-HPG5	15	79	72.5	26,681
C (85)-HPG10	14	84	122.1	44,935
A (80)-HPG5	20	80	78.2	16,312
A (80)-HPG10	17	81	125.3	26,138

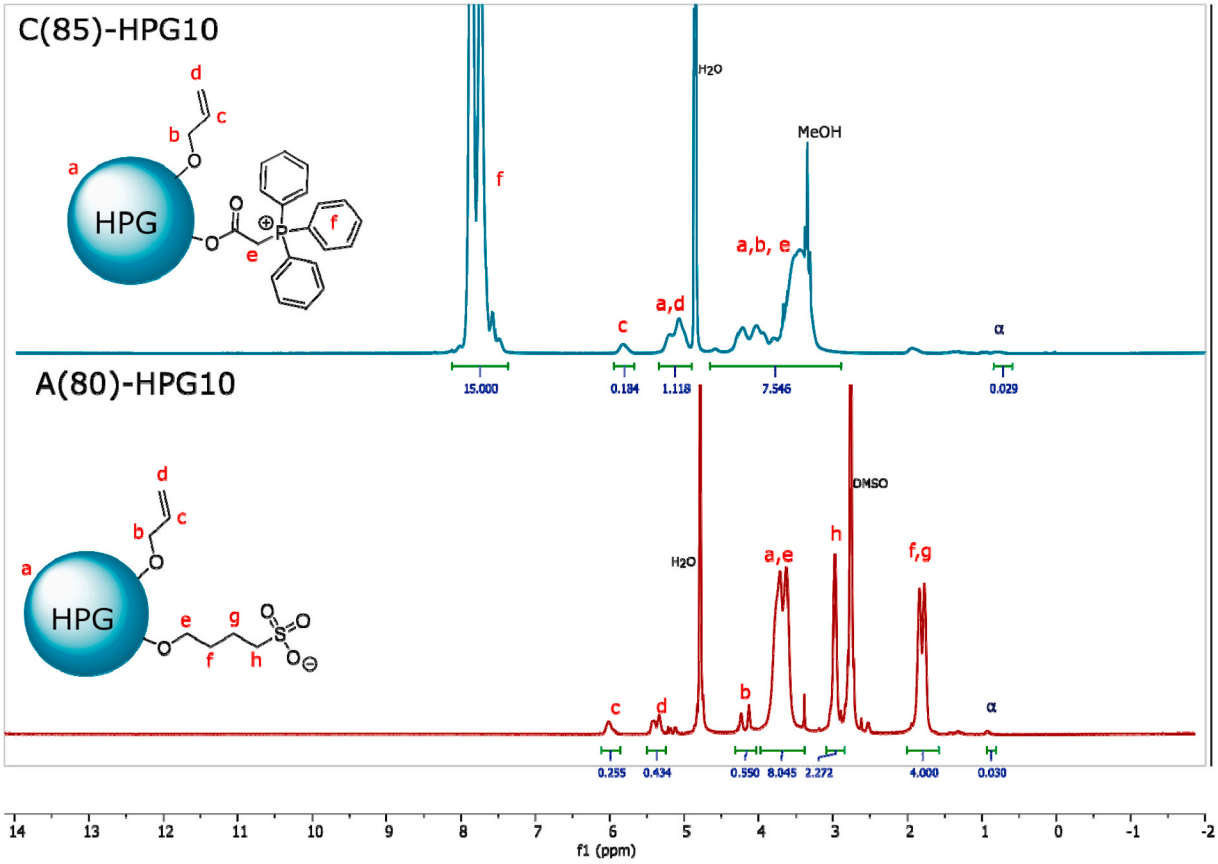

Fig. 5. H NMR of C (85)-HPG10 and A (85)-HPG10 and illustrative representation of Hyperbranched Polyglycerol structure (grey ball) and terminal functionalization of its hydroxyl (-OH) groups. α-protons indicate the single core methyl group in HPG (3H).

synthesized based on 2.5, 5, and 10 kDa HPGs with approximately 15% DF allyl groups and 55% (referred to as C (55)-HPG) or 85% (referred to as C (85)-HPG) DF cationic phosphonium. For the A (80)-HPG series, 5 and 10 kDa HPG-based electrolytes were synthesized with approximately 20% DF allyl groups and 80% DF anionic sulfonate. The amount of functional groups per polyelectrolyte (Table 2) could be estimated by comparing the summed proton signals of the functionalized HPG against the corresponding core methyl α-proton signal (Figs. 5, 6S-13). These values were in good agreement with each other and the initial hydroxyl groups/polymer (Table 2) values in the pre-functionalized HPGs. Reported M_w of the polyelectrolytes were based on each series degree of functionalization (C (55)HPG: 293.21 g/mol), C (85)HPG: 339.76 g/mol, A (80)HPG: 208.61 g/mol) and amount of functional groups.

Aggregate size distribution of the functionalized HPGs was detected via dynamic light scattering (DLS). Characteristic results from the C (85)-HPG 2.5, 5, and 10 kDa series is shown in Fig. 6. The data indicate that micelles/aggregates were formed for all three C-HPG masses and that a size-dependent formation could be observed in the radius range of 90–130 nm with larger aggregates arising from larger C-HPG (10 > 5>2.5). Lower radius modes were detected but due to the DLS detection uncertainty in these ranges the unipolymer (<10 nm) determination was not reliable. Aggregation promotion has previously been linked with charge in carboxylic HPGs and indicated an apolar core and a highly charged exterior structure conducive to forming aggregates [39].

3.4. IEM transport characterization

Cross-linked free-standing membranes (see Experimental section) were mounted in a custom H-cell between two electrolyte reservoirs (Fig. 2). As a first evaluation of the membrane properties, electrochemical impedance spectroscopy (EIS) were performed using the indirect method [30] (resistance measured with membrane minus the baseline resistance without the membrane). Impedance ionic conductivity results, with NaCl, are reported in Figure S15-16 and are summarized in Fig. 7. These results are displaying an increase in conductivity for both A-HPG and C-HPG (all formulations) versus increasing polymer size.

To further investigate this ionic conductivity trend with polymer size, direct current measurements were performed. A low constant potential (1 V) was applied between the H-cell's source and target electrodes to prevent limiting currents [10] and the target electrolyte concentration was kept constant at 10 mM. By switching the source electrolyte concentration (10, 50, 100, 200, and 400 mM), conductivity could be established by comparing the resulting steady-state currents. The results are summarized in Table 3 (and Figure S17). Again, the same ionic conductivity trend was observed with C (55)-HPG series, 10 F2 > 5 F2 > 2.5 F2 > 5 F1 (where F2 membranes contained higher amounts of C-HPG than F1). Importantly, the conductivity trend was not inversely correlated with the membrane selectivity and switching the source electrolyte to a higher concentration (compared to the target) didn't significantly increase the measured conductivity over the different membranes. This is likely due to minimal unselective "leakage" through the membranes and the conductivity results remaining limited by the lower target reservoir concentration (10 mM). C (55) F2 membranes based on 2.5 and 10 kDa HPG did however display better selectivity than the C (55)-HPG 5 membrane (Figure S17B-D).

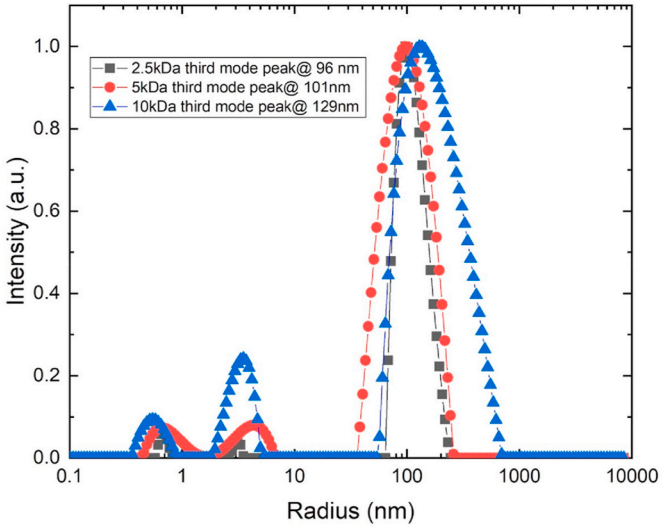

Fig. 6. Size distributions from dynamic light scattering (DLS) of C (85)-HPG series based on 2.5, 5 and 10 kDa HPG's. Major peak modes at 96, 101 and 129 nm show large aggregates/micelles formed by the polymers in size dependent order. Lower modes <10 nm is near the resolution limit of DLS and have to be interpreted carefully.

We additionally investigated the free-standing dendrolyte membranes' capabilities of transporting larger ionic species using the proxy molecule Alizarin Red S (342.25 g/mol, Fig. 3). Compared to small inorganic ions (*e.g.*, Cl^- 35.45 g/mol), the anionic Alizarin Red S molecule does not have formal charge on all of the atoms in its structure, which could results in less facile ionic movement through the IEM. Furthermore, the aromatic nature of Alizarin Red S could lead to π-π interactions with the phosphonium functionalization of the C-HPG, also contributing to less ideal ion transport. Transport was evaluated in a DC four-probe experiment using the H-cell setup and a C (55)-HPG5 F1 membrane (Figure S21). After approximately 25 min and established trend of decreasing voltage (Figure S22), the characteristic dark coloration of Alizarin Red S was observed close to the membrane interface in the target electrolyte (Figure S21, S23) demonstrating successful transportation of the large molecule. To investigate if the Alizarin Red S transport was dominated by active (electrophoretic) or passive (diffusional) transport, both the source (Alizarin Red S) and target (NaCl) electrolytes were refreshed after the active transport runs (Figure S21) and the passive diffusion of the dye into the target electrolyte was measured after 16 h with the pre-loaded membrane (Figure S23). The concentration determined for the active transport was 4 × higher (0.12 mM) compared to the passive diffusion with the pre-loaded membrane (0.03 mM). It's also important to point out that the active transport was performed over approx. 33 min while the passive transport was determined after approx. 16 h, leading to a 2 order of magnitude difference in "flow rate" (60.61 nM/s vs 0.52 nM/s, for 33 min and 16 h, respectively).

As a final investigation of the HPGs' IEM performance parameters, DC conductivity analysis were conducted using previously reported capillary-based organic electronic ion pumps (OEIPs) [10,12,19,20] (Figure S18). In such devices, the IEM takes the form of an extended channel (5 mm long, 27 μm wide, 12 μm thick) rather than the more conventional free-standing membranes as studied, see above. Conductivity values for dendrolyte-OEIPs, operated using a NaCl source electrolyte, are summarized in Table 3 (more details and other electrolyte data are given in Figure S19). Compared to the values obtained from the impedance measurements of the C (55)-HPG F2 and A (80)-HPG membranes above, OEIP DC conductivities were in general lower but the size-dependent conductivity trend remained. The differences are likely related to the micromolding processing, performed within the capillaries (MIMIC) [31], and the associated encapsulation restrictions for the membranes as compared to the more open attachment of the free-standing membranes. Even so, successful transportation of large aromatic methylene blue ions (319.85 g/mol, Fig. 3) could be performed and was visibly observed as the A-HPG membrane channel in the OEIP was being filled and colorized by the ion while running the experiment (Figure S18), thus demonstrating "large" molecular ionic transport capabilities in the anionic dendrolyte membrane with an encapsulated setup.

The fixed charge concentrations were estimated in the OEIP mem-

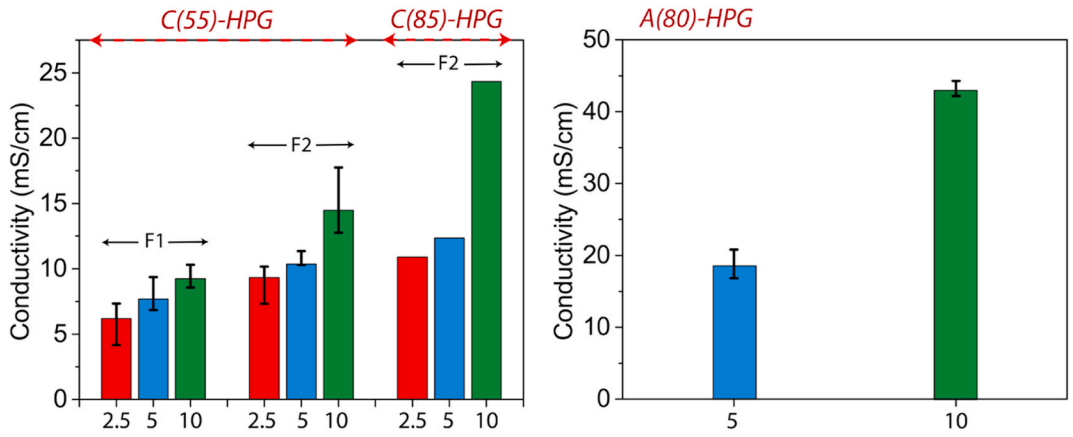

Fig. 7. Conductivity at 0.5 M NaCl (AC measurements - EIS). (Left) AEM series based on 2.5, 5 and 10 kDa sized hyperbranched polyglycerol with ~55% (C (55)-HPG) and ~85% (C (85)-HPG) functionalized cationic charges. Membrane formulation F1 series containing 47% w/w C-HPG polymer and F2 70% w/w. (Right) CEM series based on 5 and 10 kDa hyperbranched polyglycerol with 80% (A (80)-HPG) functionalized anionic charges, both membranes formulation containing 70% w/w A-HPG polymer. Increasing ionic conductivity could be seen in all series for both AEM and CEM based on the increasing polymer size (10 > 5 > 2.5 kDa HPG).

Table 3
Summary of ionic conductivity, fixed charge concentration, and degree of swelling for dendrolyte membranes. C-HPG membrane formulation F1 and F2 is based on 47% resp. 70% w/w cationic polymer content.

	Impedance (EIS) Free-standing (mS/cm at 0.5 M NaCl)[a]	DC OEIP (mS/cm at 0.1 M NaCl)	DC OEIP Fixed Charge Concentration[b] (mol/L)	DC Free-standing (normalized conductivity)[c]	Degree of Swelling (%) at 0.5 M (and 0.1 M) NaCl
C(55)-HPG5 F1	7.7			0.77	91 (125)
C(55)-HPG2.5 F2	9.3	6.2	0.28	1.00	104 (160)
C(55)-HPG5 F2	10.4	8.0	0.49	1.16	70 (108)
C(55)-HPG10 F2	14.5	10.3	0.63	2.32	61 (112)
A(80)-HPG5	18.8 (26.0 at 0.1 M)[a]	25.1	–		
A(80)-HPG10	43.2 (not possible at 0.1 M)[a]	34.7	0.74		

[a)] With measurements at lower electrolyte concentration, the membranes showcased potential of lower resistance than electrolyte solution due to high amount of charges. E.g. A (80)-HPG10 membranes were not possible to be measured at 0.1 M NaCl source electrolyte with the indirect method since it would result in a calculated negative resistance. Measurements at 0.1 M was possible for the A (80)-HPG5 membranes and the values obtained can be reliably compared with the DC OEIP;[b)] ionic-exchange with Cl^- -→ Br^- measured on cationic C (55) membranes and $Na^+ \rightarrow Li^+$ measured on anionic A (80) membranes;[c)] Conductivity measured with 0.1 M NaCl source and target electrolyte. Conductivity values measured normalized to C (55)-HPG2.5 F2.

brane channels by performing an ion-exchange of the mobile counter ions in the membranes and was calculated using [20]:

$$total\ moles\ exchanged = \frac{1}{zF}\int_{t_i}^{t_f} I(t)dt \tag{4}$$

Where z is the ionic charge number, F is the Faradays constant (96,485 C mol^{-1}), t_i and t_f are the initial and final time points of the interval between the two steady state currents $I(t)$ of the different ionic species (A → B). The fixed charge concentration is obtained by dividing the total moles exchanged (Equation (4)) with the membrane volume of the OEIP channel. The fixed charge concentrations (Table 3, Figure S20) scaled with the membrane conductivities (C-HPG 10 > 5 > 2.5).

From all these results, the conductivity-size dependant trend could be observed in all the cases, for both anionic and cationic HPG membranes, at different electrolyte concentrations, as free-standing and micro capillary membranes, in both AC and DC measurements.

3.5. Electrolyte uptake

The amount of electrolyte solution present in equilibrated free-standing membrane was calculated as the degree of swelling (DS):

$$DS(\%) = \frac{m_{wet} - m_{dry}}{m_{dry}} \times 100 \tag{5}$$

where m_{wet} is the mass of the equilibrated fully-hydrated membrane and m_{dry} is the mass of the dry membrane (previously equilibrated in deionized water). Fig. 8 shows the DS for various C-HPG formulations of 2.5, 5, and 10 kDa in electrolyte of varying concentration. In general, the DS increased with lower C-HPG polyelectrolyte content (F1 > F2) and less DS was seen with the higher degree of cationically charged polyelectrolytes (C (85) < C (55)) except in the case of C-HPG2.5 F2 series. Membrane hydration is essential for achieving efficient ionic transport and the associated active and passive (electrophoretic and diffusive) transport of hydration water [2]. Several models have been proposed to explain different ionic transport phenomena related to the microstructure in semi-permeable membranes [40]. In this study no observation was made linking an increase in the DS with lower ionic resistance in the membranes. Indeed, the more conductive membranes demonstrated lower DS. In the C (55)-HPG F2 series (Table 3), the higher amount of fixed charge concentration in the polymer membrane was associated with a lower DS, without compromising IEM selectivity (Figure S17).

Previously reported dendrolyte modelling has shown that with sufficient generations (size) there is a tendency for terminal charged groups to back-fold into the interior, suppressing the charge-charge repulsion

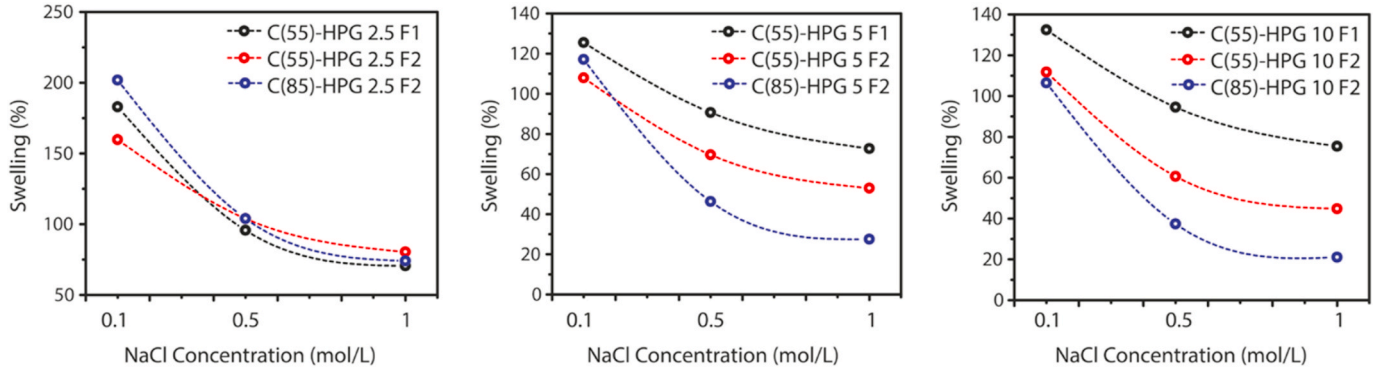

Fig. 8. Degree of swelling (electrolyte uptake) of the three series of C-HPG membranes based on 2.5, 5, and 10 kDa HPG as a function of electrolyte concentration. C (55)-HPG polymers have a lower amount of cationic phosphonium charges (~55%) than C (85)-HPG (~85%). F2 membranes comprise of a higher amount poly electrolyte content (70% w/w) compared to F1 with a lower (49% w/w) in the membrane casting solutions.

exhibited by the terminal charged groups and thus lowering the DS [41–45]. Swelling of larger dendrolytes (higher generation) was explained to occur mainly with the unfolding of densely branched structure [42,45]. The larger C-HPG5 and C-HPG10 exhibited less degree of swelling, possibly due to the back-folding phenomena, where efficient ionic condensation could occur with higher amounts of fixed charge groups without the aid of increased hydration levels.

4. Conclusions

In this study, a series of different sized HPGs (2.5, 5, and 10 kDa) were multi-functionalized using cross-linking groups and different fixed amounts of positive or negative charged groups. The final polyelectrolytes sizes were estimated via H NMR analysis and by aggregate/micelle size dependent formation in DLS. The resulting dendrolytes were cross-linked via thiol-ene click chemistry into free-standing AEMs and CEMs and the structure-property relationship between polyelectrolyte size and ionic conductivity was investigated. An increase in ionic conductivity was found to be associated with increasing the hyperbranched polyelectrolyte polymer size in IEMs. The trend was observed via both AC electrochemical impedance spectroscopy and DC ion transport experiments with NaCl (*i.e.*, Na^+ transport through CEMs and Cl^- transport through AEMs).

The increased ionic conductivity and fixed charge concentration in the membranes were found not to be correlated with an increasing degree of swelling, which points towards structural folding phenomena with the large polyelectrolyte based IEMs.

The dendrolyte HPG-based membranes demonstrate ionic conductivity with the A (80)-HPG10-based CEM yielding Na^+ conductivity up to 40–50 mS/cm (at 0.5 M NaCl, Figure S16). The AEM (C (85)-HPG10 F2) demonstrated a Cl^- conductivity of 25 mS/cm (at 0.5 M NaCl). Most IEMs are designed for applications in fuel cells, desalination, or other scenarios involving transport of small-sized ions (*e.g.*, H^+, Na^+, Cl^-). Dendrolytes demonstrated ionic transportation of larger aromatic molecular ions ($\gtrsim$ 120 g/mol). This is of particular importance when considering healthcare applications, such as those utilizing the OEIP [11,13], where electrophoretic transport can be used to deliver therapeutic substances with high spatiotemporal/dose precision for treatment epilepsy [9,46,47], pain [11], or other signaling disorders [7,8]. Even though a thorough study of large aromatic ionic molecular transport is beyond the scope of this article, two basic investigations of Alizarin Red S (342 g/mol) and methylene blue (320 g/mol) ionic transport were demonstrated in the dendrolyte membranes. With this study, the hope is to advance the understanding of ionic transport phenomena and the development of synthetic approaches – and experimental design – for more rational routes to achieve efficient ionic conductive polymer materials. For example, optimizing some of the synthesized membranes properties, such as degree of swelling, requires unforeseen optimizations in film casting and mounting. The development of commercial IEM materials, efficient cross-linking, and integrated physical support for free-standing membranes has been a decades-long undertaking. Doubtless, such efforts will also be required for dendrolyte membranes, but the structure-property relationships elucidated above, as well as the synthetic optimizations, may go a long way in facilitating this process.

Declaration of competing interest

The authors declare the following financial interests/personal relationships which may be considered as potential competing interests: Tobias Abrahamsson, Klas Tybrandt, Magnus Berggren, and Daniel T. Simon are shareholders in the small, researcher-controlled intellectual property company OBOE IPR AB (oboeipr.com), which owns patents related to this research.

Acknowledgements

T.A. acknowledges Hongli Yang (Linköping University) for help with the EIS experimental setup. We also wish to thank Alexander Minidis (RISE) and Joanna Oreskär (RISE) for helping with synthesis, characterization, and supply of HPG, and Fareed Ahmed (Linköping University) for experimental support and fruitful discussions.

N.M. acknowledges a mobility grant from the Swiss Society for Biomaterials and Regenerative Medicine, SSB + RM. Support for this research was provided by the Swedish Foundation for Strategic Research, the Swedish Research Council, and the European Union's Horizon 2020 research and innovation program under grant agreement no. 834677 (European Research Council (ERC) Advanced Grant for Magnus Berggren). This work was conducted within the frameworks of the BioCom Lab and e-NeuroPharma projects.

Appendix A. Supplementary data

Supplementary data to this article can be found online at https://doi.org/10.1016/j.polymer.2021.123664.

References

[1] G.M. Geise, H.J. Cassady, D.R. Paul, E. Logan, M.A. Hickner, Specific ion effects on membrane potential and the permselectivity of ion exchange membranes, Phys. Chem. Chem. Phys. 16 (2014) 21673–21681, https://doi.org/10.1039/C4CP03076A.

[2] K.-D. Kreuer, Ion conducting membranes for fuel cells and other electrochemical devices, Chem. Mater. 26 (2014) 361–380, https://doi.org/10.1021/cm402742u.

[3] H. Strathmann, Electrodialysis, a mature technology with a multitude of new applications, Desalination 264 (2010) 268–288, https://doi.org/10.1016/j.desal.2010.04.069.

[4] A. Oehmen, R. Viegas, S. Velizarov, M.A.M. Reis, J.G. Crespo, Removal of heavy metals from drinking water supplies through the ion exchange membrane bioreactor, Desalination 199 (2006) 405–407, https://doi.org/10.1016/j.desal.2006.03.091.

[5] R.K. Nagarale, G.S. Gohil, V.K. Shahi, Recent developments on ion-exchange membranes and electro-membrane processes, Adv. Colloid Interface Sci. 119 (2006) 97–130, https://doi.org/10.1016/j.cis.2005.09.005.

[6] Y. Tanaka, Ion Exchange Membranes: Fundamentals and Applications, second ed., Ion Exch. Membr. Fundam. Appl, 2015, pp. 1–500, https://doi.org/10.1016/C2013-0-12870-X. Second Ed. 47.

[7] D.T. Simon, S. Kurup, K.C. Larsson, R. Hori, K. Tybrandt, M. Goiny, E.W.H. Jager, M. Berggren, B. Canlon, A. Richter-Dahlfors, Organic electronics for precise delivery of neurotransmitters to modulate mammalian sensory function, Nat. Mater. 8 (2009) 742–746, https://doi.org/10.1038/nmat2494.

[8] T. Arbring Sjöström, M. Berggren, E.O. Gabrielsson, P. Janson, D.J. Poxson, M. Seitanidou, D.T. Simon, A decade of iontronic delivery devices, Adv. Mater. Technol. 3 (2018), 1700360, https://doi.org/10.1002/admt.201700360.

[9] C.M. Proctor, A. Slézia, A. Kaszas, A. Ghestem, I. del Agua, A.-M. Pappa, C. Bernard, A.J. Williamson, G.G. Malliaras, Electrophoretic drug delivery for seizure control, Sci. Adv. 4 (2018) eaau1291, https://doi.org/10.1126/sciadv.aau1291.

[10] M. Seitanidou, K. Tybrandt, M. Berggren, D.T. Simon, Overcoming transport limitations in miniaturized electrophoretic delivery devices, Lab Chip 19 (2019) 1427–1455, https://doi.org/10.1039/c9lc00038k.

[11] A. Jonsson, Z. Song, D. Nilsson, B.A. Meyerson, D.T. Simon, B. Linderoth, M. Berggren, Therapy using implanted organic bioelectronics, Sci. Adv. 1 (2015), https://doi.org/10.1126/sciadv.1500039 e1500039–e1500039.

[12] D.J. Poxson, M. Karady, R. Gabrielsson, A.Y. Alkattan, A. Gustavsson, S.M. Doyle, S. Robert, K. Ljung, M. Grebe, D.T. Simon, M. Berggren, Regulating plant physiology with organic electronics, Proc. Natl. Acad. Sci. Unit. States Am. 114 (2017) 4597–4602, https://doi.org/10.1073/pnas.1617758114.

[13] M. Seitanidou, R. Blomgran, G. Pushpamithran, M. Berggren, D.T. Simon, Modulating inflammation in monocytes using capillary fiber organic electronic ion pumps, Adv. Healthc. Mater. 8 (2019), 1900813, https://doi.org/10.1002/adhm.201900813.

[14] X. Strakosas, M. Seitanidou, K. Tybrandt, M. Berggren, D.T. Simon, An electronic proton-trapping ion pump for selective drug delivery, Sci. Adv. 7 (2021), https://doi.org/10.1126/sciadv.abd8738.

[15] I. Bernacka-Wojcik, M. Huerta, K. Tybrandt, M. Karady, M.Y. Mulla, D.J. Poxson, E. O. Gabrielsson, K. Ljung, D.T. Simon, M. Berggren, E. Stavrinidou, I. Bernacka-Wojcik, M. Huerta, K. Tybrandt, M. Karady, M.Y. Mulla, D.J. Poxson, E. O. Gabrielsson, K. Ljung, D.T. Simon, M. Berggren, E. Stavrinidou, Implantable organic electronic ion pump enables ABA hormone delivery for control of stomata in an intact tobacco plant, Small 15 (2019), 1902189, https://doi.org/10.1002/smll.201902189.

[16] H. Strathmann, Ion-exchange Membrane Separation Processes, Elsevier, 2004, https://doi.org/10.1007/s13398-014-0173-7.2.

[17] C. Hoon, C. Hyun, M.D. Guiver, Y. Moo, Progress in Polymer Science Sulfonated hydrocarbon membranes for medium-temperature and low-humidity proton exchange membrane fuel cells (PEMFCs), Prog. Polym. Sci. 36 (2011) 1443–1498, https://doi.org/10.1016/j.progpolymsci.2011.06.001.

[18] H. Frey, R. Haag, Dendritic polyglycerol: a new versatile biocompatible material, Rev. Mol. Biotechnol. 90 (2002) 257–267, https://doi.org/10.1016/S1389-0352(01)00063-0.

[19] T. Abrahamsson, D.J. Poxson, E.O. Gabrielsson, M. Sandberg, D.T. Simon, M. Berggren, Formation of monolithic ion-selective transport media based on “click” cross-linked hyperbranched polyglycerol, Front. Chem. 7 (2019) 484, https://doi.org/10.3389/fchem.2019.00484.

[20] D.J. Poxson, E.O. Gabrielsson, A. Bonisoli, U. Linderhed, T. Abrahamsson, I. Matthiesen, K. Tybrandt, M. Berggren, D.T. Simon, D.J. Poxson, et al., Capillary-fiber based electrophoretic delivery device, ACS Appl. Mater. Interfaces 11 (2019) 14200–14207, https://doi.org/10.1021/acsami.8b22680.

[21] Q. Ge, Y. Liu, Z. Yang, B. Wu, M. Hu, X. Liu, J. Hou, T. Xu, Hyper-branched anion exchange membranes with high conductivity and chemical stability, Chem. Commun. 52 (2016) 10141–10143, https://doi.org/10.1039/c6cc04930c.

[22] M. Zou, J. Fang, J. Liu, C. Li, R. Guan, Synthesis and preparation of sulfonated hyperbranched poly(arylene ether sulfone)/poly(ether sulfone) blend membranes for proton exchange membranes, Solid State Ionics 220 (2012) 23–31, https://doi.org/10.1016/j.ssi.2012.05.020.

[23] Q. Ge, X. Liang, L. Ding, J. Hou, J. Miao, B. Wu, Z. Yang, T. Xu, Guiding the self-assembly of hyperbranched anion exchange membranes utilized in alkaline fuel cells, J. Membr. Sci. 573 (2019) 595–601, https://doi.org/10.1016/j.memsci.2018.12.049.

[24] H.E. Gottlieb, V. Kotlyar, A. Nudelman, NMR chemical shifts of common laboratory solvents as trace impurities, J. Org. Chem. 62 (1997) 7512–7515, https://doi.org/10.1021/jo971176v.

[25] P.A. Hassan, S. Rana, G. Verma, Making Sense of Brownian Motion: Colloid Characterization by Dynamic Light Scattering, 2015, https://doi.org/10.1021/la501789z.

[26] F. Paulus, M.E.R. Weiss, D. Steinhilber, A.N. Nikitin, C. Schütte, R. Haag, Anionic ring-opening polymerization simulations for hyperbranched polyglycerols with defined molecular weights, Macromolecules 46 (2013) 8458–8466, https://doi.org/10.1021/ma401712w.

[27] Y. Jiang, J. Chen, C. Deng, E.J. Suuronen, Z. Zhong, Click hydrogels, microgels and nanogels: emerging platforms for drug delivery and tissue engineering, Biomaterials 35 (2014) 4969–4985, https://doi.org/10.1016/j.biomaterials.2014.03.001.

[28] C.E. Hoyle, C.N. Bowman, Thiol-ene click chemistry, Angew. Chem. Int. Ed. 49 (2010) 1540–1573, https://doi.org/10.1002/anie.200903924.

[29] L. Zhu, T.J. Zimudzi, N. Li, J. Pan, B. Lin, M.A. Hickner, Polymer Chemistry Crosslinking of comb-shaped polymer anion exchange membranes via thiol–ene click chemistry, Polym. Chem. 7 (2016), https://doi.org/10.1039/c5py01911g.

[30] A.H. Galama, N.A. Hoog, D.R. Yntema, Method for determining ion exchange membrane resistance for electrodialysis systems, Desalination 380 (2016) 1–11, https://doi.org/10.1016/j.desal.2015.11.018.

[31] E. Kim, Y. Xia, G.M. Whitesides, Micromolding in capillaries: applications in materials science, J. Am. Chem. Soc. 118 (1996) 5722–5731, https://doi.org/10.1021/ja960151v.

[32] A. Sunder, R. Hanselmann, H. Frey, R. Mülhaupt, Controlled synthesis of hyperbranched polyglycerols by ring-opening multibranching polymerization, Macromolecules 32 (1999) 4240–4246, https://doi.org/10.1021/ma990090w.

[33] D. Hölter, A. Burgath, H. Frey, Degree of branching in hyperbranched polymers, Acta Polym. 48 (1997) 30–35, https://doi.org/10.1002/(SICI)1521-4044(19990201)50:2/3<67::AID-APOL67>3.0.CO;2-W.

[34] W. Radke, G. Litvinenko, A.H.E. Müller, Effect of core-forming molecules on molecular weight distribution and degree of branching in the synthesis of hyperbranched polymers, Macromolecules 31 (1998) 239–248, https://doi.org/10.1021/ma970952y.

[35] R. Hanselmann, D. Hölter, H. Frey, Hyperbranched polymers prepared via the core-dilution/slow addition technique: computer simulation of molecular weight distribution and degree of branching, Macromolecules 31 (1998) 3790–3801, https://doi.org/10.1021/ma971197r.

[36] J.U. Izunobi, C.L. Higginbotham, Polymer molecular weight analysis by 1H NMR spectroscopy, J. Chem. Educ. 88 (2011) 1098–1104, https://doi.org/10.1021/ed100461v.

[37] R.K. Kainthan, E.B. Muliawan, S.G. Hatzikiriakos, D.E. Brooks, Synthesis, characterization, and viscoelastic properties of high molecular weight hyperbranched polyglycerols, Macromolecules 39 (2006) 7708–7717, https://doi.org/10.1021/ma0613483.

[38] D. Wilms, F. Wurm, J. Nieberle, P. Böhm, U. Kemmer-Jonas, H. Frey, Hyperbranched polyglycerols with elevated molecular weights: a facile two-step synthesis protocol based on polyglycerol macroinitiators, Macromolecules 42 (2009) 3230–3236, https://doi.org/10.1021/ma802701g.

[39] E. Barriau, H. Frey, A. Kiry, M. Stamm, F. Gröhn, Negatively charged hyperbranched polyether-based polyelectrolytes, Colloid Polym. Sci. 284 (2006) 1293–1301, https://doi.org/10.1007/s00396-006-1522-7.

[40] T. Luo, S. Abdu, M. Wessling, Selectivity of ion exchange membranes: a review, J. Membr. Sci. 555 (2018) 429–454, https://doi.org/10.1016/j.memsci.2018.03.051.

[41] R. Nikam, X. Xu, M. Ballauff, M. Kanduč, J. Dzubiella, Charge and hydration structure of dendritic polyelectrolytes: molecular simulations of polyglycerol sulphate, Soft Matter 14 (2018) 4300–4310, https://doi.org/10.1039/c8sm00714d.

[42] J.S. Kłos, J.-U. Sommer, Simulations of terminally charged dendrimers with flexible spacer chains and explicit counterions, Macromolecules 43 (2010) 4418–4427, https://doi.org/10.1021/ma1003997.

[43] P.K. Maiti, R. Messina, Counterion distribution and ζ-potential in PAMAM dendrimer, Macromolecules 41 (2008) 5002–5006, https://doi.org/10.1021/ma7025435.

[44] I.V. Mikhailov, A.A. Darinskii, Does symmetry of branching affect the properties of dendrimers? Polym. Sci. 56 (2014) 534–544, https://doi.org/10.1134/S0965545X14040105.

[45] J.S. Kłos, J.U. Sommer, Coarse grained simulations of neutral and charged dendrimers, Polym. Sci. - Ser. C. 55 (2013) 125–153, https://doi.org/10.1134/S1811238213070023.

[46] A. Jonsson, S. Inal, I. Uguz, A.J. Williamson, L. Kergoat, J. Rivnay, D. Khodagholy, M. Berggren, C. Bernard, G.G. Malliaras, D.T. Simon, Bioelectronic neural pixel: chemical stimulation and electrical sensing at the same site, Proc. Natl. Acad. Sci. Unit. States Am. 113 (2016) 9440–9445, https://doi.org/10.1073/pnas.1604231113.

[47] A.J. Williamson, J. Rivnay, L. Kergoat, A. Jonsson, S. Inal, I. Uguz, M. Ferro, A. Ivanov, T.A. Sjöström, D.T. Simon, M. Berggren, G.G. Malliaras, C. Bernard, Controlling epileptiform activity with organic electronic ion pumps, Adv. Mater. 27 (2015) 3138–3144, https://doi.org/10.1002/adma.201500482.